Equivalent circuit model of a non-faradaic impedimetric ZnO nano-crystal biosensor

John Eveness*, Lu Cao, Janice Kiely, Richard Luxton

Institute of Bio-Sensing Technology, University of the West of England,
Bristol, BS16 1QY, U.K.
*Corresponding author. Tel.: +44(0)117 32 87667; e-mail: john.eveness@uwe.ac.uk).

Abstract

This paper describes the development of an equivalent electrical circuit (EEC) model of a unique co-planar electrode PET-ZnO biosensor platform. This non-faradaic ZnO biosensor had a PET insulating layer between the electrodes and the active ZnO sensor surface and impedance spectroscopy was used to measure varying concentrations of C-reactive protein (CRP). Analysis of the impedance magnitude bode plot reveals a slope indicative of a capacitive behaviour, where R^2 is 0.99. Furthermore, extraction of the complex impedance parameters shows capacitive reactance (Xc) being the dominant parameter as a result of capacitive transduction mechanism.

The EEC was based on the generalized Randles model and adapted to represent the non-faradaic ZnO biosensor. Experimental data was fitted to the model at 100 kHz to establish values for the component parts of the biosensor system. With these values the model showed good correlation between experimental and modelled data across the frequency range studied, within the limitations of the measurement instrument. The model quantified charge modulations arising due to bimolecular binding of CRP within the electrical double layer (EDL) formed at the ZnO-PBS interface. The CRP bio-molecular interaction within the EDL can cause high charge carrier density accumulation in the semiconductor and as a result the capacitance of the EDL is increased. The EEC model quantifies this phenomenon, presented as a parallel capacitance connected to the ZnO-Antibody interfacial capacitance.

The model was adapted to two variants of the biosensor design, with differing ZnO nanoparticle concentrations forming the sensor surface. The variations on the components of the modelled concurred with expected changes established from biosensor surface analysis. Using the EEC model, the dominance of each constituent sensor element on measurement stability is quantified identifying the significant contributors to experimental and sensor-to-sensor repeatability to support control of parasitic effects.

Keywords — Electrical Impedance Spectroscopy, Biosensor, Non-faradaic, Equivalent Electrical Circuit model, polyethylene terephthalate (PET), Zinc-Oxide, PCB electrode, CRP

1.0 Introduction

Non-faradaic impedance spectroscopy (NFIS) is a powerful technique to capture subtle changes of the interaction at an electrode-electrolyte interface to measure charge modulation at the interface without the need for the redox molecule [1]. Thus, NFIS facilitates a label-free approach requiring a small AC voltage applied in a frequency sweep, allowing assay conjugations at the surface to remain unaffected [2]. Another benefit of the NFIS approach in comparison to faradaic type sensor is that typically no reference electrode is required, which simplifies the detection electronics, making it a more amenable to application in miniaturised, integrated, point-of-care devices [3][4]. Finally, the complexity of the sample preparation is reduced, as no redox probe is required [5]. While it has been reported that faradaic biosensors tend to be more sensitive [3], achieving lower limits of detection compared with a non-faradaic technique, advances in synthesis techniques have resulted in NFIS being a competitive approach in some applications. For example, not only sensitivity, but also linear range have been enhanced by applying metal oxides to create nano-textured, biocompatible surfaces on biosensor electrodes [6]. Semiconducting materials, such as zinc oxide (ZnO) nanostructures, possess functional and morphological properties that enhance sensitivity for transducing physicochemical changes associated with biomolecular binding in NFIS biosensors [2]. ZnO wurtzite nanostructures are composed of Zn^{2+} and O^{2-} ions which are stacked alternatively along the c-axis [6]. Because of the presence of zinc interstitials and oxygen vacancies, ZnO is intrinsically a n-type semiconductor material, which exhibits good electron transport properties [6]. ZnO also has a high isoelectric point (IEP ~ 9.5) and therefore at the physiological pH it is positively charged, enhancing immobilisation of negatively charged biomolecules due to their lower IEP [6]. Other advantages of the use of ZnO nanostructures are their low cost, the fact they are non-hazardous and biocompatible, plus various structures can be formed through a variety of manufacturing processes.

Depending on the method of fabrication, a diverse range ZnO nanostructures, offering various properties, can be formed. Biosensors produced from these nanostructures can be tailored to the measurement of various biomarkers. For example, ZnO nanorod structures were deposited by a simple hydrothermal method on interdigitated microelectrode transducers for immobilization of anti-horseradish peroxidase (anti-HRP) antibodies [7]. Munje et al. fabricated ZnO thin films via a pulsed laser deposition method to measure cortisol in synthetic sweat with high sensitivity (1 pg/mL in synthetic sweat and 1 ng/mL in human sweat) [8]. The maximum variation of capacitance was measured in the 5-6 KHz frequency range [8]. By contrast, Shanmugam et al. developed a biosensor for cardiac troponin (cTnT) using nanostructured ZnO sensing electrodes to create a NFIS [9]. The hydrothermal method permitted deposition of the ZnO on flexible porous polyimide substrate with the aim of producing an affordable sensor for use by patients at home. Another approach by Selvam et al. used shadow masks and a radio frequency magnetron sputtering technique to deposit gold and ZnO on rigid glass and flexible polyimide substrates, to form electrochemical sensors for quantification of Ethyl glucuronide (EtG) [10]. The ZnO sensor systems demonstrated a higher sensitivity of 0.001 µg/L compared with the gold sensor (1 µg/L) for the detection of EtG [10]. For ZnO nanoparticle based structures, the use of ultrasound assists in the dispersion of powders, fragmenting large agglomerates and avoiding subsequent aggregation. Chen et al. utilised commercial ZnO nanoparticles consisting of both strongly and weakly bonded aggregates [11]. The research team demonstrated that the fine ZnO nanoparticles, created by applying ultrasound to the ZnO in water, acted as nuclei to obtain 'flower-like' structures, which were not possible without ultrasound. Chung et al. [12] also compared the characteristics of ZnO nanoparticles in water via ultrasonic dispersion using a probe or a bath and demonstrated that the probe produce superior results in terms of the effectiveness of the ultrasonic dispersion technique.

In previous work, presented by Cao et al, the concept of synthesizing a ZnO nanoparticle substrate utilising a colloidal dispersion technique, incorporating sonication has been proven [13][14]. The advantage of this technique is that biosensor surfaces, with controlled compositions and nanostructures, could be created at low cost using standard laboratory equipment and electrical impedance spectroscopy to measure the biochemical binding of CRP at the functionalised metal-oxide surface. The technique was also scalable for large volume synthesis. A NFIS based sensor, targeting C-reactive protein (CRP) demonstrated the benefits in terms of simplifying sample preparation, as no redox probe required, and creating a simple sensor system, without the requirement for a reference electrode. C-reactive protein (CRP) can be a comparing point as a model for biosensor design. It was selected as the model antigen to demonstrate

biosensor performance. The result was a rapid measurement (10 minutes in total), and good sensitivity of less than 1 ng/ml for ZnO nanoparticles on polyethylene terephthalate **(**PET) substrates [13][14] and 27 pg/ml for a ZnO/CuO nanoparticle composite [15]. The equivalent electrical circuit (EEC) model of this biosensor structure [13] is the topic of the study described in this paper.

In order to understand the operation and predict performance of EIS biosensors, lumped impedance electrical equivalent circuit (EEC) models are frequently used. Among the existing models, the Randles equivalent circuit is the most frequently employed [16]. Using this model, the complex impedance response allows the faradaic and non-faradaic processes to be decoupled [12]. A number of authors have adapted the Randles model, producing distributed resistor and capacitor equivalent circuits. For example, to understand the influence of the ZnO electrical parameters on the sensor's performance, Jacobs et al [17] developed a model in which the dynamic ranges of the individual parameters were estimated and the simulation was compared with experimental results for two types of sputter-deposited ZnO thin films. Munje et al. [8] compared the performance of planar glass versus nano-porous substrates with a functionalised ZnO thin film to measure cortisol in synthetic sweat. The model was used to examine the sensitivity of the biosensors, confirming that the confinement of biomolecules in the nano-porous substrate caused increased charge accumulation in the electrical double layer at the ZnO–solution interface enabling small dynamic changes due to biomolecule binding to be detected. Tanak et al [2] fitted a modified Randles equivalent circuit to the impedance spectra of interdigitated gold electrodes fabricated on a flexible polyimide substrate coated with a thin film of ZnO. This showed an increase in capacitance of the electrical double layer with increasing dose concentrations caused by the capacitive binding effect at the electrode interface occurring due to antibody/antigen interaction. Selvam et al [10] used a modified Randles equivalent circuit to study the nature of the impedance spectra for the detection of Ethyl glucuronide (EtG) in human sweat. The measured impedance, identified as being non-faradaic, was dominated by the capacitance of the double layer formed at the sensing electrode-fluid interface.

The models previously described in the literature rarely consider NFIS biosensors in which an insulating dielectric layer is positioned between the electrodes and the binding surface [13] and no reports have been identified of NFIS sensors in this format, which include deposited nanoparticle-based ZnO layers on PET substrate. This approach provides the potential for a cost effective reusable or disposable point-of-care biosensor chip. Previous modelling work typically considers a semiconductor material deposited directly on to metal electrodes [2][10][17], and there are examples of electrodes being embedded within PET microfluidic channels separated from the sensing region and the use of electrical impedance measurement to quantify enzyme concentrations within a micro fluidic sample chamber [18].

The modelling work described in this paper considers the development of an EEC model of a biosensor structured as a polyethylene terephthalate (PET) insulating layer separating the electrodes from a ZnO biocompatible sensing surface. Our desired modelling approach in this work involved adaptation of the Randles circuit to provide a detailed representation of the structure of our nanoparticle impedimetric sensor. We used a novel empirical approach of building up an EEC model relating to the layers of sensor structure. This provided a deeper understanding of the sensor operation and an accurate understanding of sensor's layer-by-layer impedance contribution. We were able to identify potential dominate systematic noise sources at a sub-component level. We believe the presented results and EEC model serve as an important guide for enhancing the sensitivity of future capacitive biosensors developed by the technique described in this paper.

This paper is structured as follows. In section 2, the biosensor structure, including the electrodes, the ZnO film and the functionalised sensor surface is described, followed by the protocol for the impedance measurement of CRP. In section 3 the equivalent circuit model of the sensor system is detailed, providing an improved understanding of the sensor and a first approximation of its characteristic parameters, leading to quantification the effect of the binding interaction on the functionalised ZnO surface. Finally, the equivalent circuit model is implemented to evaluate the dominance of each constituent element of the sensor on measurement stability, giving an insight as to how the experimental conditions and biosensor

design could be optimised, with potential to improve sensing performance parameters such as accuracy, precision and sensitivity.

2.0 Biosensor structure and EEC modelling

2.1 Biosensor structure

Details of the fabrication method have been described previously [1]. The structure of the sensor consist of a co-planar D-shaped electrode formed from 35 µm copper on FR4 substrate (printed circuit board PCB). The overall diameter of the co-planar electrode is 23 mm, each electrode has a width of 11 mm and separation distance between the electrodes is 1.0mm. The sensor surface component comprises a 140 µm thick PET substrate (20mm x 20mm) on which ZnO layer is formed [13]. In this study, biosensors with two different ZnO nanocrystalline layers were evaluated; one formed from by drop-coating a suspension of 1 % concentration ZnO and a second formed using a suspension of 0.5 % ZnO. A polymer cover with a sensing aperture of 10 mm x 4 mm, exposing the ZnO biocompatible sensing surface, is positioned above the ZnO layer. The ZnO sensor chip is functionalised by 40 µl of monoclonal mouse anti-human C-reactive protein (4C28 Mab: C6) from HyTest Ltd (Turku, Finland). The CRP dose was prepared at a range of concentrations in PBS (1ng/mL, 5 ng/mL and 10 ng/mL). 75 µl of CRP solution was pipetted onto the biosensor chip, which is placed freely onto the co-planar electrode (as depicted by figure 1). The optimum sensing area is located where the electrostatic fringe-field exists, at the separation gap between the electrodes [19][20]. After an incubation period of 10 minutes, an impedance spectra measurement was performed using Cypher C60 impedance analyser for PBS (baseline) and for each concentration of CRP.

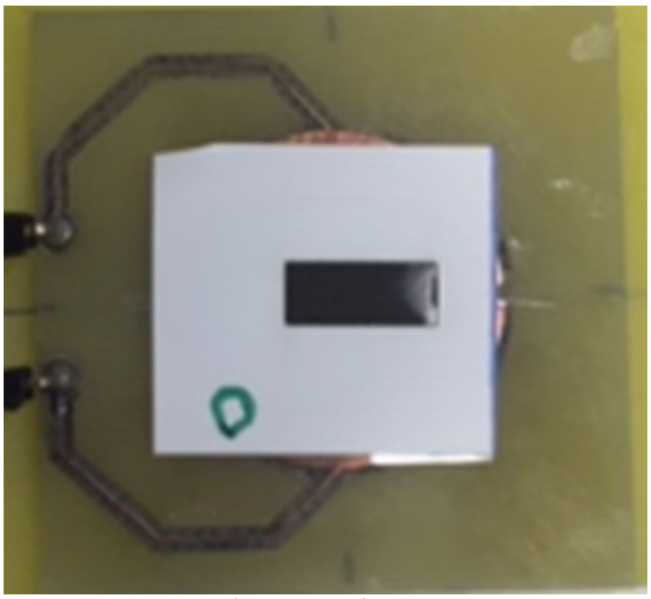

Fig. 1. Top-view image of The PET-ZnO biosensor chip positioned on the co-planar sensing electrode.

2.2 Impedance spectroscopy and measurement of CRP

A Cypher Instruments C60 Impedance-Amplitude-Phase Analyser, configured to impedance-mode measurement was used for the EIS measurements. The electrodes are insulated by PET, no DC current can flow between the electrodes and there is no redox reaction making this method non-faradaic electrical impedance spectroscopy. The C60 instrument generates a sine wave voltage excitation signal and the signal voltage across the sensor and the current flowing through the sensor are measured by the C60 at the BNC measurement plane. At this point, the voltage signal at the BNC output is the voltage across the device under test (DUT). The current flowing through the DUT is measured internally in the C60. The phase of the output voltage and current are measured relative to the internal sine wave generator. The voltage, current and phase shifts are used to calculate the complex impedance of the DUT. For open-circuit scenario the C60 reaches a maximum impedance of 455 kΩ. This is an upper impedance boundary of the unit set by the internal noise floor of the electronics. The lower impedance boundary of 10 mΩ at low frequencies is set by the BNC connector output resistance and inductance. The co-planar electrode was connected to the C60 impedance measurement BNC connector by BNC 50 Ω coaxial cable. The frequency was scanned from 10 Hz to 4 MHz at a voltage of 2 Vpp with 300 test points. A sufficient electrode voltage is needed to generate a sufficient electrostatic field beyond the PET layer in order to charge the zinc oxide substrate. Typically for applications where sensing is done at the surface of the electrode, AC signal potentials are small, generally around 10mV pk-pk. However, studies of contact free capacitive sensing where electrodes are embedded within PET channels have suggested AC signal voltages from 50 mVpp to 3 Vpp are necessary [21].

The impedance plots were analysed by Cypher Graph V1.2 impedance amplitude and phase analyser graphing application software, then imported to ZView and R for further analysis and visualisation of complex impedance components. The Modulus of Impedance |Z| spectra were recorded systematically for each constituent component of the sensor structure and assay in the following order: coax cable; bare electrode; PET, PET-ZnO surface, functionalised ZnO surface with anti-CRP antibodies, PBS baseline, and for CRP concentration of 1ng/mL, 5 ng/mL and 10 ng/mL. A CRP dose response plot and analysis of the biosensor performance has been previously reported [13].

The Impedance spectrum of the biosensor for each concentration of CRP was acquired in triplicate. Measurements were recorded after 10 minutes incubation time following the addition of 75 µl of human C-reactive protein (CRP) from HyTest Ltd. CRP was prepared at a range of concentrations: 0 (PBS baseline only), 1 ng/mL, 5 ng/mL and 10 ng/mL diluted in 0.025 M PBS with pH 7.40. The biosensors were used to evaluate the sensor response to increasing concentrations of CRP with 100 ng capture antibody and 10 minutes incubation time.

2.3 Equivalent Electrical Circuit Modelling

The circuit schematic of the Randles model describing the faradic and non-faradic processes consists of *Rs* to represent the resistance of the solution (electrolyte), in series with the interface of electrode-electrolyte modelled by *Cd or Cedl.* Where *Cd* defines the non-faradaic electrical double-layer capacitance that is connected in parallel with the faradaic impedance charge transfer resistance *Rct,* and the Warburg impedance due to diffusion of the chemical reactants in solution [22]. Other impedance elements have also been considered in the model, defining the cell's geometric material properties such as: electrode track resistance; electrode substrate material permittivity; electrolyte solution permittivity and other system parasitic elements, such as the sensor-instrument connectivity impedance all of which affects the global impedance response of the sensor [23][24]. The electrical double layer element C*dl* may sometimes also be expanded to show the contribution of the individual immunoassay elements, such as a linker molecule; capture-antibody, target antigen, and detection-antibody [25]. The ZnO biosensor is generally modelled as a two-stage resistor–capacitor circuit to define the electrical parameters that influence sensor performance. The first stage of the circuit is a resistor–capacitor combination connected in parallel, associated with the nanocrystal or nanoparticle structure of the ZnO film representing the ZnO substrate inherent resistance and capacitance. The second stage of the circuit is another resistor–capacitor combination that represents the effects of the charge accumulation and transfer due to protein biomolecules and buffer medium present

on the ZnO sensor surface and the associated electrical double layer formed at the ZnO electrolyte interface. The resistive component of this charge transfer is termed generally as *Rct*. The electrical double layer region at the liquid–metal oxide interface is represented as a capacitance, generally termed *Ced*l, which is influenced by the protein binding on the sensor surface. The charged ions in the buffer solution result in current conduction in the bulk solution, modelled as an independent resistive component, typically as Rs.

The generalized Randle's model can be adapted for modelling NFIS based biosensors, where an insulating layer is position between the electrodes. In this work, the ZnO NFIS sensor illustrated in figure 1, a Randles model-based equivalent circuit was developed. This model included impedances that represent the electrical double layer interface formed at the ZnO-PBS interface and the capacitance resulting from biochemical binding of antigen at the ZnO nano-crystal sensor surface, as well as an impedance for the bulk PBS electrolyte. Building on the Randles model, the intrinsic impedance of the PET-ZnO sensor substrate and that of the electrode PCB support material were also included. The model of a NFIS biosensor omits the Randles components of the charge transfer resistance and Warburg impedance. These elements are not characteristic of NFIS, particularly capacitive type sensors, and in particular, the technique described in this paper where the sensing electrodes are separated from the active sensing surface by a dielectric substrate. For modelling purposes a symmetrical system is assumed.

Complex parameters Zimg (Xc) and Zreal (R) for each constituent element of the biosensor system and for a CRP concentration of 10 ng have been systematically fitted to the measured complex impedance response at 100 kHz. Analysis of complex impedance parameters at this frequency allows us to decouple and quantify the biosensor's global characteristic impedance response to the target antigen from that of the impedance associated with sensor-to-instrument connectivity and the instrument's upper impedance boundary. By systematically extracting measured complex impedance parameters *Zimg* (*Xc*) and *Zreal* (*R*) for each constituent component of the sensor structure, a comprehensive EEC model of the sensor system based on a CRP concentration of 10 ng can be constructed and simulated to calculate the modulus of impedance and phase angle using Analog Devices LTspice® circuit simulator software.

Analysis of the measured complex impedance parameters were carried out, negligible contributors to the impedance response were omitted from the resultant equivalent circuit model. The model's response was validated by comparing the modulus of impedance |Z| to that of the measured (average) impedance spectra at frequencies between 3 kHz to 4 MHz, To understand origins of compound error affecting experimental and sensor-to-sensor repeatability, the model was implemented to simulate the modulus of impedance output variation, by systematically applying 10% tolerance to each component value. The resulting impedance error value is calculated, ranking the dominance of each constituent component of the sensor

3 Results and discussion

3.1 Impedance spectroscopy measurement of CRP

The results of the EIS measurements in the form of impedance magnitude Bode plots of CRP concentrations from 1 ng/mL to 10 ng/mL in PBS and complex impedance parameters (Zimg, Zreal) extracted at 100 kHz are shown in Figure 2. Figure 2a displays modulus of impedance |Z| over the frequency range of 10 Hz to 4 MHz. Analysis of the impedance spectra given in figure 2a over the frequency range 10 kHz to 4 MHz reveals a slope where R^2 is 0.99. This is indicative of a capacitive behaviour and reinforces the assumption that it is appropriate to represent the biosensor behaviour as purely capacitive. An R^2 value less than 0.99 would have meant that it would be more appropriate to model it as a constant phase element component (CPE), representing a non-ideal capacitor [18] [26]. As the frequency decreases to approximately 10 kHz the measured impedance magnitude begins to curve, then at 1 kHz the impedance response begins to flatten. This is an artefact originating from the fact that the impedance |Z| of the biosensor that is connected as a parallel impedance load to the C60's measurement plane heads towards the instruments upper impedance boundary. Below approximately 1 kHz the impedance response flattens despite the fact that the biosensor impedance |Z| is actually greater than that of the upper impedance boundary of the instrument. Within the frequency range below 1 kHz, any increase in capacitive loading is measured as a decrease in impedance from the C60's upper impedance boundary of 450 kΩ [27]. Figure

2b shows a magnified section of impedance magnitude spectra from 90 kHz to 120 kHz, showing clearly the impedance decreasing for an increase in CRP concentration. Electrochemical impedance spectroscopy (EIS) can be used to measure an electrical double layer (EDL) formed when a semiconducting material interacts with liquid electrolytes [6][28]. ZnO has a high isoelectric point (pI) of approximately 9.5, which makes it suitable for absorption of relatively negatively charged proteins, e.g. enzymes and antibodies with lower pI's, primarily driven by electrostatic interaction. The net charge on the molecule is affected by pH of its surrounding environment and can become more positively or negatively charged due to the gain or loss, respectively, of protons (H^+). In this experimental set-up, ZnO is positively charged, whereas the CRP is dominated by net negative charge (pI of CRP is ~5.45) in the physiological strength media (in this experiment pH is 7.3). When a protein, in this case CRP-antibody is immobilized on a solid surface and binds to it's analyte CRP-antigen, a protein–analyte complex is formed. The change in conformation leads to an increase in molecular size of a protein–analyte complex. This increase in size of a protein–analyte complex therefore leads to a relatively large permanent dipole moment (larger the difference in electronegativity, the larger the dipole moment) [29][30]. When CRP antigen binds to the ZnO surface through capture by the receptor antibody, a decrease in the absolute impedance value due to a decrease in the overall positive charge with increasing CRP loading is measured (fig 2b). The EIS results indicate that there is increased negative charge accumulation due to the effect of bound antigen's net charge. Thus, a decrease in the overall positive charge with increasing CRP-antigen loading is measured. This concurs with literature, which reports that changes in the surface dielectric and charge distribution are induced when a protein target binds to the receptor previously attached to the electrode, displacing water and ions from the surface [4][31]. Analyte size and net charge must be considered when designing the biosensor through charge modulation within the EDL when measuring non-faradaic changes Most commonly, the Debye length is matched to or larger than the size of the binding biomolecules [32]. However, some authors have recognised that measurement can still be performed beyond the Debye length where there is still an electric potential gradient[33]. The molecular weight and the estimated scale of CRP on the basis of the protein data bank is 116 kDa, 10 × 10 × 4 nm. The anti-CRP antibody isotype is polyclonal IgG. The IgG size is 151 kDa, 16 × 5 × 5 nm. Therefore, in this sensor development, we are sensing the antibody-antigen interaction beyond a distance of the Debye length from the nanoparticle/solution interface. Consequently, the calculated Debye length at the CRP concentrations is approximately 1.9 nm for 25 mM (5x dilution) PBS. The Debye length is expected to be non-uniform due to zinc oxide nano crystal formation.

Figure 2c displays the complex impedance parameters Zimg (Xc) and Zreal (R) at 100 kHz. Extraction of the complex impedance parameters presented by figure 2c reveals capacitive reactance (Xc) being the sensor's dominant transduction mechanism to CRP binding to the ZnO nanocrystal surface. The results show a decrease in capacitive reactance (Xc) as a result in capacitive loading for increase in CRP concentration.

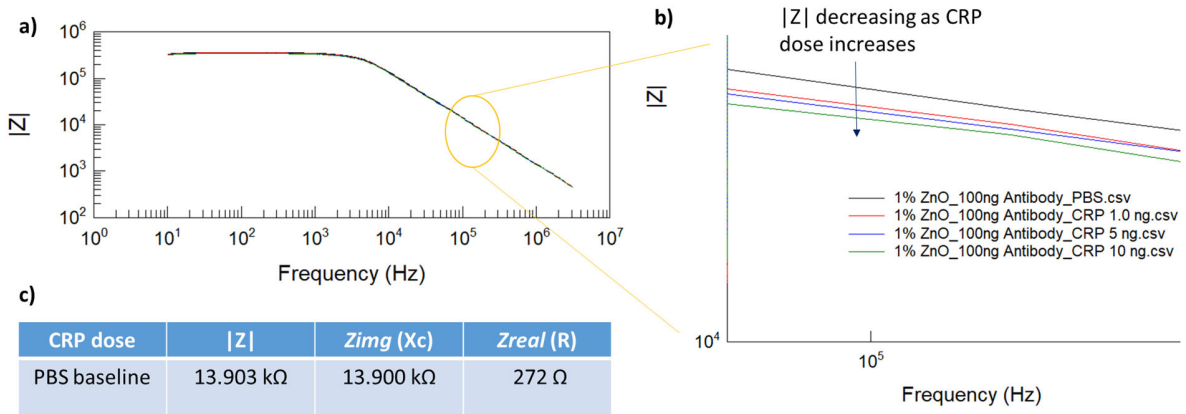

c)

CRP dose	|Z|	*Zimg* (Xc)	*Zreal* (R)
PBS baseline	13.903 kΩ	13.900 kΩ	272 Ω
1 ng/mL	13.603 kΩ	13.600 kΩ	297 Ω
5 ng/mL	13.503 kΩ	13.500 kΩ	304 Ω
10 ng/mL	13.403 kΩ	13.400 kΩ	304 Ω

Fig. 2. EIS measurements of CRP concentrations of 1 ng/mL to 10 ng/mL in PBS a) Bode impedance magnitude |Z| measurement at each concentration: PBS (baseline), 1 ng/mL, 5 ng/mL and 1 0 ng/mL b) magnified |Z| region 90 KHz to 120 KHz showing CRP dose response and c) complex impedance parameters (*Zimg* (Xc) and *Zreal* (R)) extracted at 100 KHz

3.2 Equivalent Electrical Circuit Model

The EEC model builds on the Randle's model adapted for the unique properties associated with the non-faradaic sensor described in the paper. The aim is to enhance the understanding of the biosensor operation to guide future biosensor development. Since the EIS bode response is complex containing impedance response of the sensor and associated impedance of the analyser's it was not to possible to fit a standard model by traditional means of EEC modelling by least square approximation. It is necessary to take a different approach. This approach is based on decomposing the EIS global response to extract the complex impedance values associate with each constituent part of the sensor to give a comprehensive equivalent circuit model, related to the Randle's circuit for a non-faradic sensor. This method allows for an identical EEC model to be fitted to the empirical data, being a more robust and appropriate method of modelling such complex EIS data. This giving a true understanding of the sensor's response to antigen binding at the surface, decoupled from that of impedance response associated with system impedance and interactions associated with underlying substrates and sensor connectivity and that of the instrument.

To understand the origin of the sensor's global impedance response to CRP and to demonstrate the sensing mechanism, the impedance magnitude |Z| at 100 kHz is obtained graphically. The purpose of the plots in figure 3 are to show the dependency of the sensor's impedance magnitude on each constituent sensor component and assay. It is evident there is a correlation in relative impedance shift as each constituent part of the sensor is systematically introduced. Figure 3b and 3c show the complex impedance parameters Xc and R. It is evident that the capacitive reactance, Xc, shown is figure 3b, is the dominant parameter contributing to the magnitude of impedance |Z|.

It is observed that ZnO deposited and dried on the PET substrate tends to increase the impedance, caused by increase reactance (Xc) due to a decrease in capacitance. The ZnO sensor surface is functionalised by 40 µl (2.5 ng/µl) of monoclonal mouse anti-human C-reactive protein (4C28 Mab: C6) and Anti-CRP antibodies (8C72). Introducing buffer onto the functionalised sensor surface forms an interfacial impedance component, contributing to an increase in capacitance. Increase CRP binding at the sensor surface decreases capacitive reactance (figure 3b) inferring that the interfacial capacitance is increasing. By deconstructing the global impedance in a manner demonstrated by figure 3, a comprehensive EEC model of the sensor system can be developed that fits the measured (average) global impedance magnitude |Z| response.

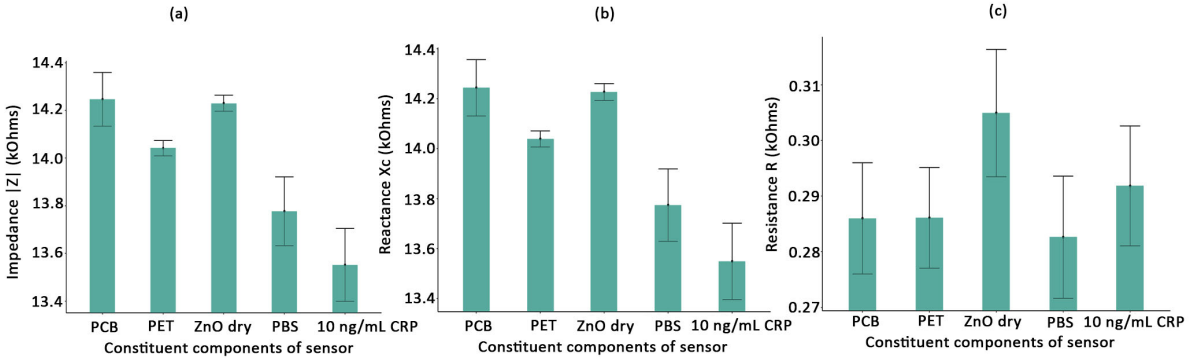

Fig 3. Deconstruction of the global impedance response |Z|. Fig 3a) displays the impedance magnitude |Z| (average n=3, Stdev error) at 100 kHz for each constituent component of the sensor system: bare PCB electrode; PET substrate; ZnO nano-crystal layer on PET; 75 uL PBS droplet on ZnO-Ab functionalized surface and CRP concentration 10 ng/mL. Fig 3(b) displays Zimg (reactance, Xc) at 100 kHz for each constituent component of the sensor, and fig 3(c) displays Zreal (R).

An illustration of the constituent components and elements of the biosensor and the corresponding equivalent circuit structure is shown in figure 4a and figure 4b respectively. Where table 1.0 tabulates the impedance component values calculated and fitted at 100 kHz for each of the physical and electrochemical components of the sensor structure. Figure 4c shows a EEC model of the C60's front-end impedance parameters and the coax cable impedance (C_{coax}). The C60 has a fixed driving impedance (52 Ω resistor) and the BNC connector $R_{contact}$, L_{BNC}, and C_{BNC} components. The lower impedance boundary is set by the output resistance $R_{contact}$ (BNC contact resistance) and inductance L_{BNC} (23 nH). This is normally a 10 mΩ resistive boundary at low frequencies. The output capacitance of the C60 (C_{BNC}) is 3 pF.

The frequency spectra generated by the model are validated by overlaying the simulated modulus of impedance |Z| response for both 1% (figure 5a) and 0.5% (figure 5b) ZnO nanocrystal substrate on the experimental impedance modulus response for the frequency range 10 Hz to 4 MHz. The model's modulus of impedance is calculated (by LTspice® circuit simulator software) in the frequency interval from 3 KHz and 4 MHz. At 10 KHz, both 1% and 0.5% ZnO models' responses, being capacitive, begin to diverge from the measured response and head towards very high impedance, above that of the open circuit impedance of the analyser. The model was however proved to have an identical response to that of the measured data over the frequency range 10 kHz to 4 MHz (Fig 5). Below, 10 KHz, the models simulated response, being capacitive, diverged from that of the measured response, heading towards very high impedance above that of the open circuit impedance of the analyser, as you would expect for a characteristic capacitive response. However, in practice within the frequency range below 10 kHz, any increase in capacitive loading is measured by the C60 instrument as a decrease in impedance relative to the C60's upper impedance boundary of 455 kΩ. In spite of the model not exhibiting identical behaviour to the measured impedance response below approximately 10 kHz, the model does however predict the actual response of the

biosensor within the lower frequency range 10Hz to 5 kHz. This method of modelling allows for decoupling from the sensor's impedance spectra response from the characteristic open circuit impedance response of the C60, demonstrating a robust and superior technique of EEC modelling for such complex EIS data. The equivalent circuit model for the 1% and the model extracted for 0.5% ZnO sensors demonstrate the same equivalent circuit structure and simulated modulus of impedance spectra trend (shown in table 1.0). It has been demonstrated by a previous study [13] how 1% ZnO sensor enhances sensitivity to CRP when compared to the 0.5% ZnO sensor. 1% ZnO offers increased binding sites and adsorption of capture antibody, increasing available sites for binding of the target CRP. This was partially due to differences in surface roughness and also due to the fact that for the 0.5% ZnO sensor there were many areas in the surface where there were deep pits revealing the underlying PET, again reducing the potential for charge accumulation [13]. The 0.5% ZnO model reveals a higher inherent ZnO capacitance (*Czno*) in series with the PET substrate capacitance but lower electrical double layer capacitance (*Czno+ab_EDL*) and lower CRP binding capacitance (*Ccrp*), approximately half the capacitance value compared to the 1% ZnO sensor. We postulate that, the higher ZnO concentration amplifies the electrical double layer charge accumulation capacity [6], demonstrated by a higher EDL capacitance, it is more sensitive to the modulation of the EDL caused by antibody/antigen binding capacitance (C*crp*) when target protein binds to the capture antibody bound to the ZnO surface.

The PCB FR4 and PET substrates are considered as dielectric materials having relative permittivity, μr, of 4.7 and 3.4 respectively [34]. These materials contribute to the total geometric capacitance of the co-planar electrodes. The substrate is a dielectric, expressed by a pure capacitive element [24]. For the electrode fabricated on a dielectric substrate, the capacitance is best approximated by a co-planar capacitance model [35][36]. The geometric capacitance *Cpcb* for the D-electrodes is estimated to be 3 pF. The equivalent geometric capacitance of the PET substrate which constitutes *Cpet*-zno is calculated by the same formula [36] and is approximated to be 2 pF. PET and FR4 PCB substrate being dielectric has a high intrinsic resistance greater than 10^6 Ω, presenting a very high parallel resistive path, so only the intrinsic capacitance of this material is dominant within the frequency range we are operating. The electrode and connecting track rresistance is an insignificant value of 0.2 Ω but included in the model to illustrate the distribution of system components relative to each electrode node. RG58c/u 50 Ω impedance coaxial cable has a capacitance of 100 pF/m. These estimated parameters give baseline approximations for the expected impedances related to the sensor's physical structure which have been validated by experimental measurement. The coax connection is a significant parasitic contributor to the global modulus of impedance of the sensor. This is further investigated in section 3.3.1 where analysis of the dominance of each component of the sensor system on measurement stability is tested. The current experimental set-up is that of a two-terminal EIS measurement scheme [37]. To minimise the dominance of the coax connection and other surrounding parasitic environmental effects, several design practises could be explored. The sensor could be mounted close to the instrument's measurement plane, thus reducing the length of cable or directly connecting the sensor electrode PCB to the BNC output. It may also be an advantage to ensure the surrounding media is relatively constant in terms of electrical permittivity and is shielded from all close proximity electrical influences. Conversion from the two-terminal to a four-terminal connection scheme would mitigate parasitic effects associated with instrument-sensor connection [37]. The four-terminal configuration can reduce the effects of lead impedances and contact resistances because the signal current path and the voltage sensing leads are independent. The voltage sensing leads do not detect the voltage drop caused by the impedance on the current leads [37]. However, each of these approaches increases the complexity of the measurement system, which can impact on how the sensor can be utilised. Hence, the particular importance of modelling the sensor to establish whether relevant dose dependent changes can be identified using the relative simple sensor system design.

PET substrate placed between the two electrodes forms a parallel capacitance connection to that of the PCB substrate capacitance. When ZnO is deposited and buffer solution is added to the surface we would have expected also PET capacitance connection from each electrode to the ZnO layer. However, this equivalent circuit form would present a parallel capacitance load causing the impedance to decrease further, which is not represented by the measured impedance response when ZnO is deposited on PET. By extracting a model directly from the impedance data we actually found the interaction between ZnO on PET substrate forms a series equivalent capacitance between the two electrodes as shown in figure 4a represented by components Cpet and Czno. Furthermore, adding value of EEC modelling to reveal

equivalent electrical interactions between materials for the novel biosensor arrangement we present in this paper. The impedance response of the ZnO deposited on the PET substrate shows a similar behaviour that to that of a ZnO metal-insulator-semiconductor capacitor in depletion mode [38][39]. When the depletion region of the semiconductor increases with increasing positive bias voltage, a greater negative charge builds-up in the semiconductor, thus the capacitance decreases and can be represented by an equivalent capacitance of the semiconductor presented in series to the insulator capacitance [40].

The ZnO-Antibody interfacial impedance is quantified as several pico-Farads, modelled as a series connection with the PBS electrolyte capacitance. The PBS solution complex impedance parameters, C*pbs* and R*pbs* are then effectively screened by the sensor's interfacial impedance. For completeness, the bulk PBS impedance is calculated and modelled as a parallel connected R*pbs* and C*pbs*. This part of the model is analogous to other studies regarding insulated contact-free biosensors [18][41][42] whereby the bulk electrolyte solution impedance is presented in series with the interfacial impedance resulting in a characteristic impedance slope (R^2 value between 0.99-1.0) across the measurement frequency spectra. The *x5* dilution PBS buffer bulk capacitance and resistance approximated as 12.5pF and 200 Ω respectively. The bulk capacitance *Cpbs* within the sensing region can be approximated by calculation for a co-planar electrode [36] where the buffer medium antigen concentration is small and can have a μr of 80, i.e. close to that of water [24]. $Rpbs$ originates from the finite conductivity of the solution, σ. To simplify, R*pbs* can be approximated by a system with two parallel plates electrodes [24] of area A, separated by a distance d is given by (eq 1).

$$Rpbs = d / (\sigma A) \qquad \text{(eq 1)}$$

The conductivity σ is related to the ionic concentration by eq 2.

$$\sigma = c\,(\mu p + \mu n) \qquad \text{(eq 2)}$$

Where μp and μn are respectively the ionic conductivities of the dominant positive and negative ions in the solution and *c* is the concentration of ions. In our experiments, x1 PBS buffer stock (Oxiod™) contains 137mmol/L of the dominant NaCl ions. The conductivity σ of the PBS stock solution calculated based on the conductivity of dominant positive ion (Na^+ 50.1 Scm^2/mol) and negative ion (Cl^- 76.4 Scm^2/mol) and is approximated to be 17.33 mS/cm^2 and resistance is 38 Ω. A 1:5 dilution PBS resistance *Rpbs* (eq 1) approximated to be 200 Ω.

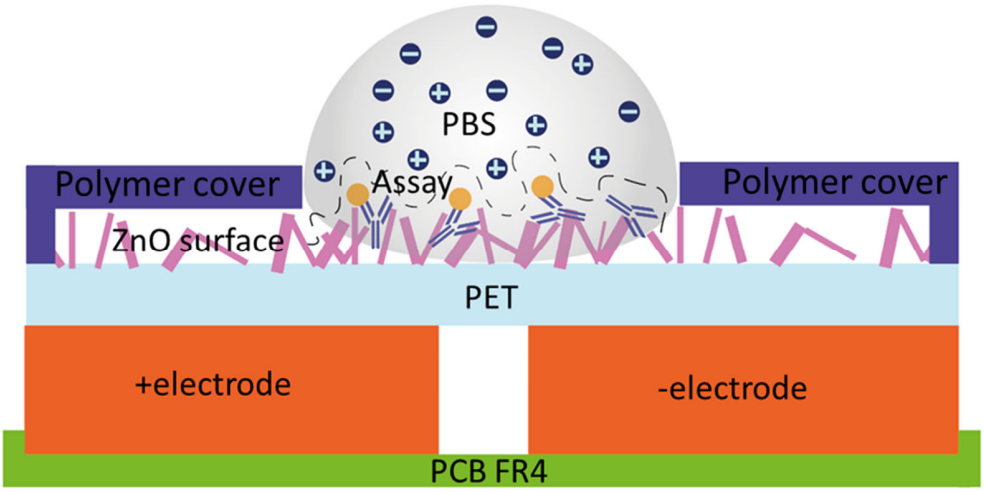
PBS
Assay
Polymer cover
Polymer cover
ZnO surface
PET
+electrode
-electrode
PCB FR4

a)

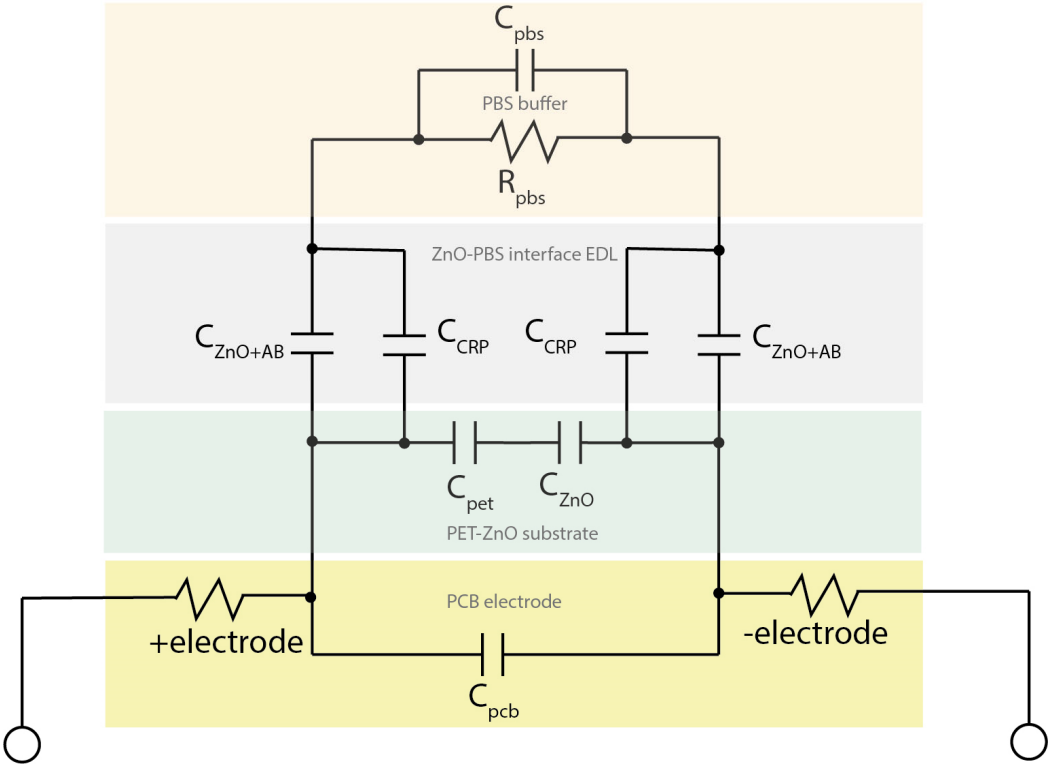
C pbs
PBS buffer
R pbs
ZnO-PBS interface EDL
C ZnO+AB
C CRP
C CRP
C ZnO+AB
C pet
C ZnO
PET-ZnO substrate
PCB electrode
+electrode
-electrode
C pcb

b)

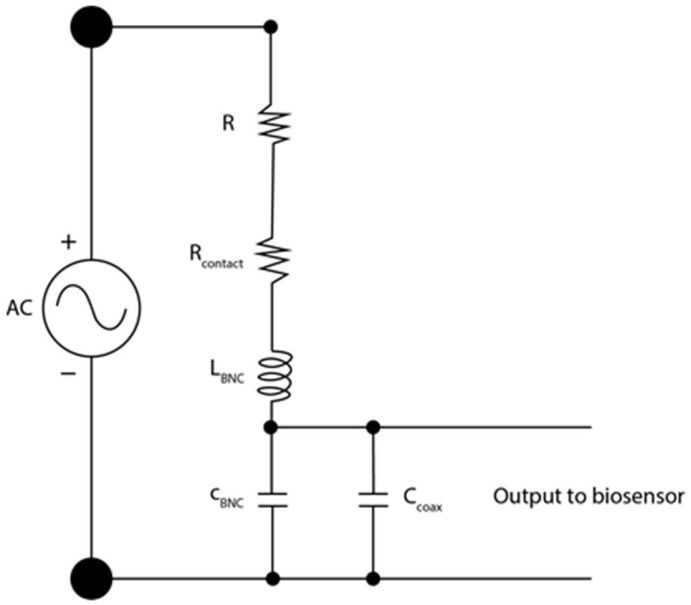

c)

Fig. 4 a) Schematic representation of the NFIS ZnO biosensor, b) EEC for the ZnO nanoparticle biosensor modelling the constituent layers of the biosensor: PCB electrode, PET-ZnO substrate, antibody functionalised ZnO in contact with PBS, bound CRP antigen and finally the bulk PBS buffer solution and fig 4c) Electrical circuit model representing the C60 instrument front-end impedance components and coax cable connection to the biosensor.

Table 1.0: Calculated and model fitted values (at 100 kHz) representing each physical component of the biosensor and electrochemical quantities of the interfacial impedance: PBS buffer solution and the lower and upper concentrations of CRP.

EEC model component	**Equivalent circuit reference**	**Calculated value**	**1% ZnO model fitted value**	**0.5% ZnO model fitted value**
Coax	C_{coax}	100 pF	104.5 pF	104.5 pF
PCB electrode	C_{pcb}	3.0 pF	4.2 pF	4.2 pF
PET substrate	C_{pet}	2.0 pF	2.0 pF	2.0 pF
ZnO substrate	C_{zno}	-	0.15 pF	2.4 pF
Bulk PBS	R_{pbs}	200 Ω	200 Ω (calculated)	
	C_{pbs}	12.4 pF	12.4 pF (calculated)	
ZnO-Ab-PBS interface	C_{ZnO+AB}	-	7.4 pF (3.7 pF total)	5 pF (2.5 pF total)
1 ng CRP	C_{CRP}	-	3 pF (1.5 pF total)	1.5 pF (0.75 pF total)
10 ng CRP		-	3.8 pF (1.9 pF total)	1.8 pF (0.9 pF total)

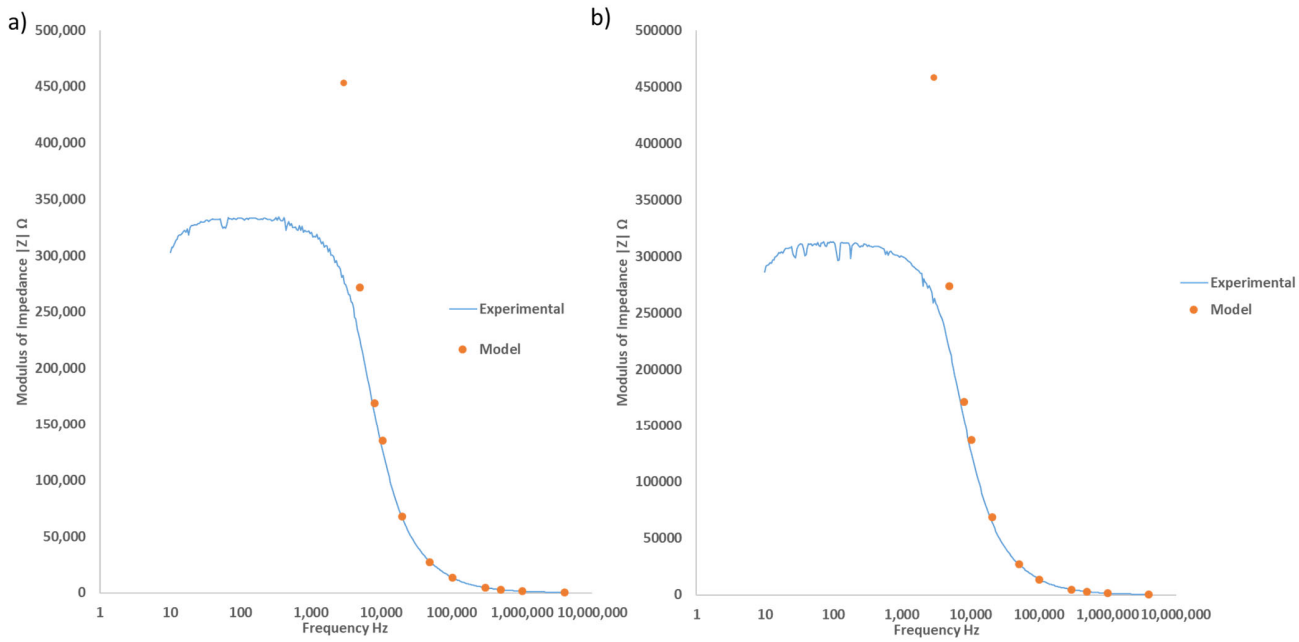

Fig. 5. Measured average impedance modulus |Z| and model's simulated impedance modulus |Z| spectra overlay for 10 ng/mL CRP. For two variants of the biosensor, Fig 5a) 1% ZnO concentration and fig 5b) 0.5% ZnO concentration sensor.

An EDL, formed when a charged semiconducting material interacts with liquid electrolytes, can have a significantly high charge carrying capacity, as high as 8.0×10^{14} cm^{-2} at ionic liquid/solid interfaces [8]. It is reported for ZnO biosensors that the EDL capacitance formed at the sensor-electrolyte interface can be in the order of nano-Farads to micro-Farads [2][8][9][17]. In our study, we have quantified the capacitance for the antibody functionalized ZnO-ionic buffer interface to be in order several pico-Farads (3.7pF, table 1.0) and is therefore dominant over the series connected ionic bulk buffer solution capacitance. Previous work [13] reported 1% concentration of ZnO demonstrated full coverage of the surface, having the largest surface area quantified as having the greatest roughness index. We speculate that an EDL formed at the ZnO surface exists and its charge capacity is dependent on a non-uniform complex crystalline formation of the ZnO, causing a varying EDL thickness distributed across the ZnO surface. The electrical double layer capacitance formed at the ZnO electrolyte interface may well be dominated by the antibody receptor interfacial capacitance connected in series, thus leading to a decrease in interfacial capacitance [31]. It is also realistic to consider that the separation distance of the ZnO biocompatible surface from the electrode by the PET dielectric substrate which will cause attenuation of the electric field strength relative to the electrode surface.

The bio-molecular interaction within the EDL can cause high charge carrier density accumulation in the semiconductor and as a result the capacitance of electrical double layer is increased from a baseline measurement [2][8]. The EEC model shown in figure 4 and table 1.0 quantify this phenomenon as a capacitive sensing mechanism, quantified as changes to the EDL formed at the ZnO semiconductor-PBS interface. Larger concentrations of target antigen in a sample will result in a greater amount of molecular interaction at the EDL, resulting in greater changes in the relative dielectric permittivity, which for a NFIS sensor contributes to the increase in interfacial capacitance, presented by the EEC model as a parallel capacitance connected to the ZnO-Antibody interfacial capacitance. Consequently, the total interfacial capacitance is the accumulative effect of the functionalized ZnO nanoparticles surface and bound antigen. It can be written as:

$$C_{total} = C_{ZnO+AB} + C_{CRP} \qquad \text{(eq 3)}$$

3.3 Simulation analysis of measurement stability

Overall, the aim is minimise measurement error, improve biosensor reproducibility and to achieve amplified sensing mechanism by increasing the sensitivity to charge modulations of the electrical double layer formed at the ZnO-electrolyte solution interface as antigen binds to the functionalised surface. Using the model in figure 4, a simulated sensor response to quantify the dominance of each sensor parameters as a contributor to measurement stability has been undertaken. Table 2.0 provides the simulated modulus of impedance |Z| output as result of systematically applying sensor component variation of 10%. The dominance of each constituent component of the sensor are listed in rank order: 1) coax cable connectivity, 2) PCB dielectric capacitance, 3) ZnO-AB interfacial capacitance, 4) CRP binding at the surface, 5) PET-ZnO capacitance, and finally 6) PET substrate capacitance. As expected, the volume PBS solution electrical parameters resistivity and capacitance have no effect on the measurement. Discussed in section 3.2, the series connected dominant interfacial EDL capacitance effectively screens the bulk PBS solution impedance.

Table 2.0. The impedance |z| dependency on variation of sensor equivalent electrical component value simulated at 100 kHz.

Rank	component	Nominal value	Nominal |Z| kΩ	component value +10%	|Z| kΩ	Δ|Z| Ω
1	C_{coax}	104.5 pF	13.552	114.95 pF	12.440	-1107
2	C_{pcb}	4.2 pF		4.62 pF	13.503	-48.30
3	C_{ZnO+AB}	7.4 pF		8.14 pF	13.509	-42.56
4	C_{CRP}	3.8 pF		4.18 pF	13.530	-21.89
5	C_{ZnO}	0.15 pF		0.165 pF	13.551	-1.49
6	C_{pet}	2 pF		2.2 pF	13.552	-0.14
insignificant	R electrode	0.2 Ω		0.22 Ω	13.552	0
insignificant	R_{pbs}	200 Ω		220 Ω	13.552	0
insignificant	C_{pbs}	12.4 pF		13.64 pF	13.552	0

Variation of inherent parasitic impedances and reproducibility of depositing and functionalising the ZnO sensor surface can effect measurement compound error and global impedance stability. Future work could explore optimising the sensor design to increase the sensitivity and precision to achieve lower limits of detection through improved control and reproducibility of the sensor fabrication and functionalisation process. If required, the instrument-to-sensor connection could be designed to minimise the signal variation associated with the most dominant parasitic component in the two-wire measurement scheme, or to explore the use of a 4-wire impedance measurement scheme to negate the connectivity impedance. The co-planar PCB electrode design used for all the experimental measurements means the PCB electrode substrate's dielectric permittivity is fixed and constant. Further work to establish true sensor performance parameters, such as experimental precision, is required for example by performing serial additions of CRP on a single PET-ZnO sensor chip. This would give a fixed and consistent PET-ZnO dielectric constant and surface topology to establish true sensor performance parameters.

Developing an EEC model by the method described in this work allows an accurate understanding of sensor's layer-by-layer impedance contribution and dominance of each constituent sensor component on the global impedance response to antigen binding at the surface. The benefit being, we were able to identify potential dominate systematic noise sources at a sub-component level, having potential to cause poor reproducibility that could be better controlled in future sensor designs. This leading to a biosensor system design exhibiting enhanced sensitivity to non-faradaic interfacial changes due to antigen binding at the sensor surface, which we have found to be in the order 10^{th} pF over the measuring range 1-10 ng. Knowing the level of resolution required will also better guide the design choice of measurement device. We believe the presented results and EEC model serve as an important guide for the development future capacitive biosensors fabricated by a facile, low-cost technique described in this paper.

4.0 Conclusions

In this study, the physical structure of a non-faradaic impedance spectroscopy-based biosensor and its complex impedance response have been examined. The sensor under study was formed from ZnO nanoparticles deposited on a PET substrate above D-shaped electrodes and was functionalized to target C-reactive protein (CRP). The results of the EIS measurements in the form of impedance magnitude Bode plots shows a decreasing dose dependent impedance magnitude response to increasing CRP concentrations. The results show a decrease in capacitive reactance (Xc) as a result of capacitive loading for increase in CRP concentration.

A comprehensive electrical equivalent circuit (EEC) model of the sensor system has been developed and fitted to the experimental data by decomposing the global impedance spectrum to reveal the impedance contribution of each constituent component of the sensor. This study has provided an improved understanding of the sensor function, by characterising the sensor's physical structure in terms of its equivalent circuit elements and enabled the decoupling of the sensor response to target antigen (CRP) from that of the characteristic impedance of the measurement instrument and parasitic elements, demonstrating the predicted properties of a non-faradaic impedance spectroscopy sensor. Biochemical binding of CRP antigen causing charge modulations at the ZnO-PBS interface is quantified by the model as a capacitive sensing mechanism and is shown to be dependent on the concentration of ZnO.

The EEC model simulation revealed good correlation between the measured and simulated results down to a frequency of 10 kHz, where the instruments upper impedance boundary is reached. The dominance of each of the sensor's physical and biochemical electrical parameters on impedance measurement stability has been evaluated by simulation analysis to identify dominant components and to support control of parasitic effects. Various technical solutions could be explored to minimize and control parasitic effects. However, approaches that are more complex could increase the complexity of the measurement system, which can impact on how the sensor can be utilised. Hence, the particular importance of modelling the sensor to establish whether relevant dose dependent changes can be identified using the relative simple sensor system design.

Future work will investigate modelling of adaptations of the sensor, including new sensor materials and structures, as well as new impedance measurement methodologies.

Author contributions

Richard Luxton and Janice Kiely conceived the original concept, funding acquisition and provided supervision and resources. Lu Cao contributed to the manuscript, immunoassay methodology, carried out the experimental investigation and initial analysis of the data. John Eveness wrote the original draft of the manuscript, contributed to data analysis, interpretation, visualisation and carried out modelling and simulation work. Richard Luxton and Janice Kiely reviewed and edited the draft and sanctioned the final version of the manuscript.

References

[1] P.M. Biesheuvel, J.E. Dykstra, The difference between Faradaic and Nonfaradaic processes in Electrochemistry, (2018) 1–10. http://arxiv.org/abs/1809.02930.

[2] A.S. Tanak, B. Jagannath, Y. Tamrakar, S. Muthukumar, S. Prasad, Non-faradaic electrochemical impedimetric profiling of procalcitonin and C-reactive protein as a dual marker biosensor for early sepsis detection, Anal. Chim. Acta X. 3 (2019) 100029. https://doi.org/10.1016/j.acax.2019.100029.

[3] R.A. Dorledo de Faria, L.G. Dias Heneine, T. Matencio, Y. Messaddeq, Faradaic and non-faradaic electrochemical impedance spectroscopy as transduction techniques for sensing applications, Int. J. Biosens. Bioelectron. 5 (2019) 29–31. https://doi.org/10.15406/ijbsbe.2019.05.00148.

[4] J.S. Daniels, N. Pourmand, Label-free impedance biosensors: Opportunities and challenges, Electroanalysis. 19 (2007) 1239–1257. https://doi.org/10.1002/elan.200603855.

[5] A.K. Assaifan, J.S. Lloyd, S. Samavat, D. Deganello, R.J. Stanton, K.S. Teng, Nanotextured Surface on Flexographic Printed ZnO Thin Films for Low-Cost Non-Faradaic Biosensors, ACS Appl. Mater. Interfaces. 8 (2016) 33802–33810. https://doi.org/10.1021/acsami.6b11640.

[6] N.R. Shanmugam, S. Muthukumar, S. Prasad, A review on ZnO-based electrical biosensors for cardiac biomarker detection, Futur. Sci. OA. 3 (2017) FSO196--FSO196. https://doi.org/10.4155/fsoa-2017-0006.

[7] P. Sanguino, T. Monteiro, S.R. Bhattacharyya, C.J. Dias, R. Igreja, R. Franco, ZnO nanorods as immobilization layers for interdigitated capacitive immunosensors, Sensors and Actuators B-Chemical. 204 (2014) 211–217. https://doi.org/10.1016/j.snb.2014.06.141.

[8] R.D. Munje, S. Muthukumar, A.P. Selvam, S. Prasad, Flexible nanoporous tunable electrical double layer biosensors for sweat diagnostics, Sci. Rep. 5 (2015). https://doi.org/Artn 14586 10.1038/Srep14586.

[9] N.R. Shanmugam, S. Muthukumar, S. Prasad, Ultrasensitive and low-volume point-of-care diagnostics on flexible strips - a study with cardiac troponin biomarkers, Sci. Rep. 6 (2016). https://doi.org/Artn 33423 10.1038/Srep33423.

[10] A.P. Selvam, S. Muthukumar, V. Kamakoti, S. Prasad, A wearable biochemical sensor for monitoring alcohol consumption lifestyle through Ethyl glucuronide (EtG) detection in human sweat, Sci. Rep. 6 (2016). https://doi.org/Artn 23111 10.1038/Srep23111.

[11] C. Chen, Q. Li, M. Nie, H. Lin, Y. Li, H. Wu, Y. Wang, An efficient room-temperature route to uniform ZnO nanorods with an ionic liquid, Mater. Res. Bull. 46 (2011) 888–893. https://doi.org/10.1016/J.MATERRESBULL.2011.02.017.

[12] S.J. Chung, J.P. Leonard, I. Nettleship, J.K. Lee, Y. Soong, D. V Martello, M.K. Chyu, Characterization of ZnO nanoparticle suspension in water: Effectiveness of ultrasonic dispersion, Powder Technol. 194 (2009) 75–80. https://doi.org/10.1016/J.POWTEC.2009.03.025.

[13] L. Cao, J. Kiely, M. Piano, R. Luxton, Facile and inexpensive fabrication of zinc oxide based bio-surfaces for C-reactive protein detection, Sci. Rep. 8 (2018). https://doi.org/10.1038/s41598-018-30793-z.

[14] L. Cao, J. Kiely, M. Piano, R. Luxton, A copper oxide/zinc oxide composite nano-surface for use in a biosensor, Materials (Basel). 12 (2019). https://doi.org/10.3390/ma12071126.

[15] L. Cao, J. Kiely, M. Piano, R. Luxton, Nanoparticle-based 3D membrane for impedimetric biosensor applications, Bioelectrochemistry. 136 (2020) 107593. https://doi.org/https://doi.org/10.1016/j.bioelechem.2020.107593.

[16] S.S. Ghoreishizadeh, X. Zhang, S. Sharma, P. Georgiou, Study of Electrochemical Impedance of a Continuous Glucose Monitoring Sensor and its Correlation With Sensor Performance, IEEE Sensors Lett. 2 (2017) 1–4. https://doi.org/10.1109/lsens.2017.2778248.

[17] M. Jacobs, S. Muthukumar, A. Panneer Selvam, J. Engel Craven, S. Prasad, Ultra-sensitive electrical immunoassay biosensors using nanotextured zinc oxide thin films on printed circuit board platforms, Biosens. Bioelectron. 55 (2014) 7–13. https://doi.org/10.1016/j.bios.2013.11.022.

[18] M. Kechadi, J. Gamby, L. Chaal, B. Saidani, B. Tribollet, Free contact microchannel impedance through two antiparallel planar microelectrodes, J. Flow Chem. 3 (2013) 81–86. https://doi.org/10.1556/JFC-D-13-00006.

[19] X. Hu, W. Yang, Planar capacitive sensors - Designs and applications, Sens. Rev. 30 (2010) 24–39. https://doi.org/10.1108/02602281011010772.

[20] F.R. Castiello, J. Porter, P. Modarres, M. Tabrizian, Interfacial capacitance immunosensing using interdigitated electrodes: the effect of insulation/immobilization chemistry, Phys. Chem. Chem. Phys. 21 (2019) 15787–15797. https://doi.org/10.1039/C9CP02129A.

[21] M. Faure, M. Kechadi, B. Sotta, J. Gamby, B. Tribollet, Contact Free impedance methodology for investigating enzymatic reactions into dielectric polymer microchip, Electroanalysis. 25 (2013) 1151–1158. https://doi.org/10.1002/elan.201200488.

[22] E.P. Randviir, C.E. Banks, Electrochemical impedance spectroscopy: An overview of bioanalytical applications, Anal. Methods. 5 (2013) 1098–1115. https://doi.org/10.1039/c3ay26476a.

[23] Kuschner, 乳鼠心肌提取 HHS Public Access, Physiol. Behav. 176 (2017) 139–148.

https://doi.org/10.1016/j.physbeh.2017.03.040.
[24] P. Dak, M.A. Alam, Non-Faradaic Impedance Model of a Biochemical Sensor, (2015) 1–14.
[25] A.P. Selvam, A. Wangzhou, M. Jacobs, T. Wu, C. Mohan, S. Prasad, Development and validation of an impedance biosensor for point-of-care detection of vascular cell adhesion molecule-1 toward lupus diagnostics, Futur. Sci. OA. 3 (2017). https://doi.org/10.4155/fsoa-2017-0047.
[26] M.E. Orazem, N. Pébère, B. Tribollet, Enhanced Graphical Representation of Electrochemical Impedance Data, J. Electrochem. Soc. 153 (2006) B129. https://doi.org/10.1149/1.2168377.
[27] Cypher, Impedance Analyser Cypher C60 System - User Manual, (n.d.).
[28] R. Beranek, (Photo)electrochemical methods for the determination of the band edge positions of TiO 2-based nanomaterials, Adv. Phys. Chem. 2011 (2011) 80–83. https://doi.org/10.1155/2011/786759.
[29] A. Quershi, Y. Gurbuz, W.P. Kang, J.L. Davidson, A novel interdigitated capacitor based biosensor for detection of cardiovascular risk marker, Biosens. Bioelectron. 25 (2009) 877–882. https://doi.org/10.1016/j.bios.2009.08.043.
[30] L. Li, C. Li, Z. Zhang, E. Alexov, On the dielectric “constant” of proteins: Smooth dielectric function for macromolecular modeling and its implementation in DelPhi, J. Chem. Theory Comput. 9 (2013) 2126–2136. https://doi.org/10.1021/ct400065j.
[31] A. Santos, Fundamentals and Applications of Impedimetric and Redox Capacitive Biosensors, J. Anal. Bioanal. Tech. S7 (2014). https://doi.org/10.4172/2155-9872.s7-016.
[32] K.C. Lin, B. Jagannath, S. Muthukumar, S. Prasad, Sub-picomolar label-free detection of thrombin using electrochemical impedance spectroscopy of aptamer-functionalized MoS2, Analyst. 142 (2017) 2770–2780. https://doi.org/10.1039/c7an00548b.
[33] G. Palazzo, D. De Tullio, M. Magliulo, A. Mallardi, F. Intranuovo, M.Y. Mulla, P. Favia, I. Vikholm-Lundin, L. Torsi, Detection beyond Debye’s length with an electrolyte-gated organic field-effect transistor, Adv. Mater. 27 (2015) 911–916. https://doi.org/10.1002/adma.201403541.
[34] M. Kechadi, L. Chaal, V. Vivier, B. Tribollet, J. Gamby, Electrical impedance spectroscopy of a PET chip sandwiched between two disk electrodes: Understanding the contribution of the polymer/electrode interface, Phys. Chem. Chem. Phys. 18 (2016) 20583–20590. https://doi.org/10.1039/c6cp03042d.
[35] J.M. Martinis, R. Barends, A.N. Korotkov, Calculation of Coupling Capacitance in Planar Electrodes, (2014) 1–5. http://arxiv.org/abs/1410.3458.
[36] Clayton R. Paul, Analysis of Multiconductor Transmission Lines, 2nd ed., Wiley, 2008.
[37] Agilent Impedance Measurement Handbook A guide to measurement technology and techniques, (n.d.).
[38] R. Ondo-Ndong, H. Essone-Obame, Z.H. Moussambi, N. Koumba, Capacitive properties of zinc oxide thin films by radiofrequency magnetron sputtering, J. Theor. Appl. Phys. 12 (2018) 309–317. https://doi.org/10.1007/s40094-018-0309-9.
[39] M.A. Dominguez, A. Orduña-Diaz, Fully solution-processed zinc oxide MIS capacitors by ultrasonic spray pyrolysis in air ambient, J. Appl. Res. Technol. 15 (2017) 278–282. https://doi.org/10.1016/j.jart.2017.01.015.
[40] L. Smith, Surface Characterization Of Thin Film Zno Capacitors By Capacitance-voltage Measurements, (2007).
[41] M. Kechadi, L. Chaal, V. Vivier, B. Tribollet, J. Gamby, Finite element modelling of non-faradic electric impedance spectroscopy through flexible polymer microchip, J. Electroanal. Chem. 807 (2017) 203–212. https://doi.org/10.1016/j.jelechem.2017.11.022.
[42] M. Kechadi, B. Sotta, L. Chaal, B. Tribollet, J. Gamby, A real time affinity biosensor on an insulated polymer using electric impedance spectroscopy in dielectric microchips, Analyst. 139 (2014) 3115–3121. https://doi.org/10.1039/c4an00212a.